CHEMISTRY
A EUROPEAN JOURNAL

ChemPubSoc
Europe

DOI: 10.1002/chem.201202341

Mapping the Metal Positions inside Spherical C_{80} Cages: Crystallographic and Theoretical Studies of $Ce_2@D_{5h}$-C_{80} and $Ce_2@I_h$-C_{80}

Lai Feng,*[a, b] Mitsuaki Suzuki,[b] Naomi Mizorogi,[b] Xing Lu,[b] Michio Yamada,[b] Takeshi Akasaka,*[b] and Shigeru Nagase*[c]

Abstract: The dynamic positions of the dimetallic cluster inside the mid-sized spherical cages of C_{80}–C_{82} have been seldom studied, despite the high abundance of $M_2@C_{2n}$ ($2n = 80$, 82) species among various endohedral metallofullerenes. Herein, using crystallographic methods, we first unambiguously map the metal positions for both $Ce_2@D_{5h}$-C_{80} and $Ce_2@I_h$-C_{80}, showing how the symmetry or geometrical change in cage structure can influence the motional behavior of the cluster. Inside the D_{5h} cage, the primary cerium sites have been identified along a cage belt of the contiguous hexagons, which suggests the significant influence of such a cage motif on endohedral cluster motion. Further analysis revealed a distorted D_{5h} cage owing to the "punch-out" effect of cerium atoms. The consequence is the presence of two localized electrostatic potential minima inside the cage of $(D_{5h}$-$C_{80})^{6-}$, thus reflecting the primary ionic cerium–cage interaction. In contrast, a different motional behavior of Ce_2 cluster was observed inside the I_h cage. With the major cerium sites, the molecule of $Ce_2@I_h$-C_{80} presented an approximate D_{2h} configuration. With the combined theoretical study, we propose that the additional unidentified influence of Ni^{II}(OEP) (OEP = octaethylporphyrin) might be also relevant for the location of cerium sites inside the I_h cage.

Keywords: crystal engineering · density functional calculations · fullerenes · host–guest systems · X-ray diffraction

Introduction

Endohedral metallofullerenes (EMFs) are created by putting a metallic atom or cluster inside a fullerene cage. These molecules, which have been proven to combine fullerene-like properties with metallic properties, have promising applications in the fields of material science and medicines.[1] Recently, dimetallofullerenes $M_2@C_{2n}$ have attracted particular interest because of their unique electronic properties and potential for use in molecular electronics.[2] However, for a better understanding of the intrinsic properties of these dimetallofullerenes, their structural elucidations are essential. To date, X-ray crystallography has been widely used for such a purpose because of its high reliability in determining not only the cage structure but also the dynamic positions of the endohedral cluster.[3] Consequently, the metal–cage and metal–metal interactions can be probed further.

Summarizing recently published crystallographic results, it appears that the metal positions of dimetallofullerenes are very dependent on the cage size and cage shape. For instance, it has been demonstrated that those cages with either super large or small size tend to contain a highly constrained dimetallic cluster. Very typical are $Sm_2@D_{3d}(822)$-C_{104},[4] $La_2@D_5(450)$-C_{100},[5] and $La_2@D_2(10611)$-C_{72}.[6] In all these cases, the cages are tubelike or ellipsoidal, which allows the dimetallic cluster to sit along the longest cage axis. It is noteworthy that each metal of the dimetallic cluster adopts an oxidation state of 2+ or 3+ because of the metal-to-cage electron-transfer interaction. This enables the two metallic cations to be separated as far as possible and therefore there is reduced mutual electrostatic repulsion between two cations. In addition, a similar trend was observed for $Sm_2@D_2(35)$-C_{88}, $Sm_2@C_1(21)$-C_{90}, and $Sm_2@D_3(85)$-C_{92},[7] which possess large and ellipsoidal cages. As revealed by their X-ray analysis, although multiple samarium positions have been identified inside the cage, the major samarium sites were found along or near the longest cage axis.

In contrast, in the mid-sized spherical cages of C_{80}–C_{82}, the dimetallic cluster is expected to fluctuate more. As for previously reported $Er_2@C_s(6)$-C_{82} and $Er_2@C_{3v}(8)$-C_{82},[8] up to 23 erbium sites with different fractional occupancies were identified in each case. In particular, inside the C_s-C_{82} cage, the major erbium sites were found along the band of ten contiguous hexagons, whereas inside the C_{3v}-C_{82} cage, it was

[a] Prof. Dr. L. Feng
Jiangsu Key Laboratory of Thin Films and School of Energy
Soochow University, Suzhou 215006 (P.R. China)
E-mail: fenglai@suda.edu.cn

[b] Prof. Dr. L. Feng, M. Suzuki, Dr. N. Mizorogi, Dr. X. Lu, Dr. M. Yamada, Prof. Dr. T. Akasaka
Life Science Center of Tsukuba Advanced Research Alliance
University of Tsukuba, Tsukuba 305-8577 (Japan)
Fax: (+81) 29-853-6409
E-mail: akasaka@tara.tsukuba.ac.jp

[c] Prof. Dr. S. Nagase
Fukui Institute for Fundamental Chemistry
University of Kyoto, Kyoto 606-8103 (Japan)
E-mail: nagase@ims.ac.jp

Supporting information for this article is available on the WWW under http://dx.doi.org/10.1002/chem.201202341.

not possible to conclude whether or not the erbium ions congregate along the similar cage band because of the disorder in cage orientation according to the authors. Regarding another mid-sized spherical cage of C_{80}, although there have been many crystallographic reports on functionalized $M_2@I_h$-C_{80} (M = La, Ce),[9] the motional behaviors of dimetallic cluster inside the pristine I_h cage and its isomeric D_{5h} cage remain unexplored. However, these behaviors shall be different from those in the functionalized I_h cage, which might be strongly disturbed or affected by those appending moieties.

In this work, we present unambiguously for the first time the X-ray crystallographic results of not only $Ce_2@I_h$-C_{80} but also $Ce_2@D_{5h}$-C_{80}. More important is the comparison study on the different motional behaviors of the Ce_2 cluster inside the isomeric C_{80} cages, which might be helpful in understanding the mutual influence between the motional cluster and cage structures.

Results and Discussion

Both of the isomers of $Ce_2@C_{80}$ were cocrystallized with Ni^{II}(OEP) (OEP = octaethylporphyrin) by using an interfacial diffusion method. Crystallographic refinement gave rise to structural determinations for $Ce_2@D_{5h}$-C_{80} and $Ce_2@I_h$-C_{80}. As shown in Figure 1, $Ce_2@D_{5h}$-C_{80} is depicted together

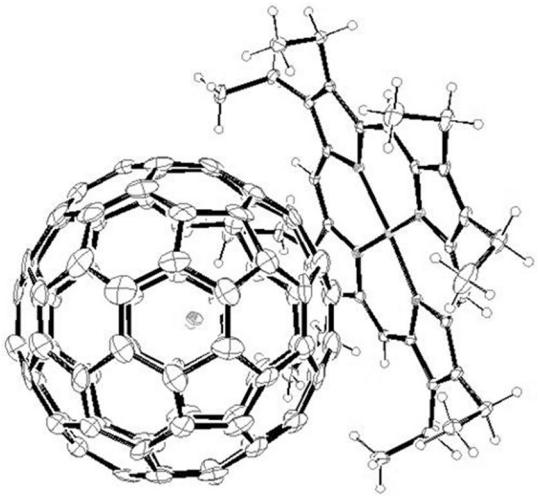

Figure 1. Drawing of $Ce_2@D_{5h}$-C_{80} and its relationship to Ni^{II}(OEP). Thermal ellipsoids at the 30% level are shown for non-hydrogen atoms. The major cerium sites Ce1A and Ce2 are nearly overlapped in this view. Solvent molecules are omitted for clarity.

with an adjacent Ni^{II}(OEP). Specifically, the D_{5h}-C_{80} cage is fully ordered, whereas several disordered cerium positions were clearly identified. Only the two primary cerium sites, labeled Ce1A and Ce2, are shown in Figure 1. Solvate molecules are omitted for clarity. The Ni^{II}(OEP) was found to be approximate to a corannulene unit of a D_{5h}-C_{80} cage with the shortest nickel-to-cage (Ni–C7A) distance of 2.804(9) Å. This value is in the expected range and similar to those of the contacts between Ni^{II}(OEP) and trimetallic nitride clusterfullerenes $M_3N@D_{5h}$-C_{80} (M = Sc, Tb, Tm).[10]

Figure 2 portrays the disordered positions of cerium sites inside the D_{5h}-C_{80} cage. The Ce sites labeled "A" are generated by the crystallographic mirror plane. Considering the

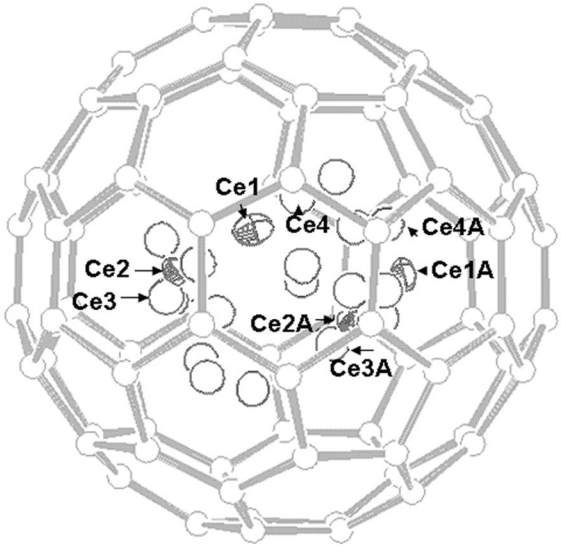

Figure 2. Drawing of $Ce_2@D_{5h}$-C_{80} showing the locations of the various partially occupied cerium sites inside the cage. Those Ce atoms labeled "A" are generated by the crystallographic mirror plane. Occupancies of major cerium sites are the following: Ce1 0.355(3), Ce2 0.278(5), Ce3 0.106(5), and Ce4 0.079(3). The occupancies of additional nine cerium sites are the following: Ce5 0.030(3), Ce6 0.029(1), Ce7 0.011(3), Ce8 0.046(4), Ce9 0.021(3), Ce10 0.028(3), Ce11 0.013(3), Ce12 0.026(3), and Ce13 0.005(2). The sum of the occupancies of all these cerium sites including those labeled A is 2.0, whereas the cage occupancy is 0.5.

ratio between the occupancies of metal and cage, only half of the cerium sites correspond to the cage with the orientation depicted in Figure 2, whereas others belong to another cage with symmetry-related orientation. However, from the viewpoint of crystallography, it is impossible to identify these cerium sites with respect to the cage orientation. For instance, the two highest occupied cerium sites, Ce1 and Ce2, actually reflect two clusters with reasonable Ce–Ce distance, which are differently positioned relative to the cage and are designated as Ce1–Ce2 and Ce1–Ce2A, respectively, in Figure 2. These two clusters are either within or intersect the plane that is aligned along the band of ten contiguous hexagons. To identify which cluster is favored with respect to the cage, we performed single-point energy calculations for the two conformers that are varied only in terms of their cluster positions. Some variation is seen in their relative energies. In particular, the conformer that contains the Ce1A–Ce2 cluster is 45.6 kcal mol^{-1} more stable than the conformer that contains the Ce1–Ce2A cluster. Consequently, the preferable cluster positions relative to the cage can be further elucidated through combined calculations. Each primary cerium site lies under a hexagonal ring. The Ce–C

distances range from 2.290(10) to 2.753(13) Å, whereas the respective Ce-to-ring centroid distances are 2.109 and 2.050 Å. Apparently, these Ce-to-cage contacts closely resemble an η^6 geometry. Another two cerium sites, Ce3 and Ce4A, which have occupancies that range from 0.11 to 0.08, were found close to the respective major cerium sites of Ce2 and Ce1A. Together, these four cerium sites represent up to 82% cerium content. Therefore, we can reasonably propose that at our applied measurement temperature (i.e., 90 K) the Ce_2 cluster undergoes a constrained motion along the cage belt of ten contiguous hexagons. This might confirm the previous NMR spectroscopic studies, which suggested more random cluster motion along the same cage belt at room temperature.[11] Despite the motional state, a wide Ce–Ce separation up to 3.764 Å is observed. This value is a little shorter than the calculated Ce–Ce distance of 3.814 Å in the D_{5h}-C_{80} cage.[11] Moreover, nine additional cerium sites have been identified inside the cage, thus indicating the possibility that the cerium atom can jump to multiple sites even at low temperature. However, these minor cerium sites together represent only 18% cerium content and have not been further identified relative to the cage.

To gain further insight into the metal–cage interaction, we calculated the electrostatic potentials of hexa-negatively charged D_{5h}-C_{80} on the basis of the X-ray structure of $Ce_2@D_{5h}$-C_{80}. The results are mapped in Figure 3a, in which

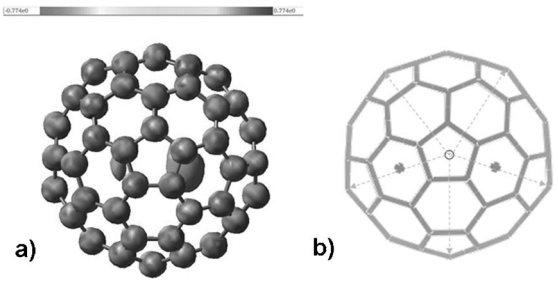

Figure 3. Electrostatic potential map of a) $(D_{5h}\text{-}C_{80})^{6-}$ and b) the view of $Ce_2@D_{5h}$-C_{80} showing the locations of Ce1A and Ce2 sites. Both are viewed from the same direction. The fivefold axis of the cage passes through the centroids of the central five-membered rings and perpendicular to the plane of this page. The dashed lines show the cage radii. The radius is defined as the distance from the cage centroid to the carbon of the 6:6 junction of the perylene unit that is along the band of ten contiguous hexagons.

the electrostatic potential distribution is polarized and two localized minima are readily recognized, which represents a remarkable electrostatic barrier to the free cluster rotation. Nevertheless, this differs from the previous theoretical result, which revealed a delocalized electrostatic potential minimum along the cage belt of ten contiguous hexagons for the DFT-optimized $(D_{5h}\text{-}C_{80})^{6-}$ and suggested a free 2D rotation of the Ce_2 cluster.[11] We assigned this difference to the small configurational variation between the cages that were constructed by means of different methods. As shown in Figure 3b, the defined radii of the D_{5h}-C_{80} cage range from 4.261 to 4.081 Å. In particular, the average radius in which the close contacts to Ce occur is 4.225(27) Å, whereas the average value of other six radii is 4.096(15) Å. Also, the carbon atoms that are close to Ce have generally higher p-orbital axis vector (POAV) values[12] relative to others (see Figure S1 in the Supporting Information). Apparently, the cage of $Ce_2@D_{5h}$-C_{80}, which is determined by X-ray diffraction analysis, is slightly "punched out" because of the encapsulation of the Ce_2 cluster and is distorted from the cage with fully optimized coordinates. Furthermore, by comparing the X-ray structure of $Ce_2@D_{5h}$-C_{80} (Figure 3b) with this potential map (Figure 3a), it was found that the major cerium sites are near the localized electrostatic potential minima, which is indicative of the primary ionic interaction between the metal atom and the cage.

$Ce_2@I_h$-C_{80} cocrystallized with Ni^{II}(OEP) in the same space group of $C2/m$, whereas an orientational disorder in the I_h-C_{80} cage was observed. Figure 4 shows only the cage

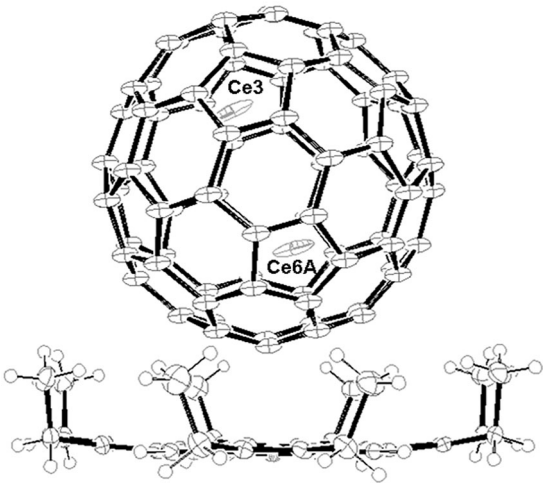

Figure 4. Drawing of $Ce_2@I_h$-C_{80} and Ni^{II}(OEP) with 30% probability displacement ellipsoids for non-hydrogen atoms. Only the cage with symmetric orientation is shown. In this view, the crystallographic mirror plane is on the plane of the page and symmetrically bisecting the present cage. The Ce3–Ce6A separation is 3.767(6) Å. Site Ce6A is generated from site Ce6 by means of the crystallographic mirror plane. The occupancies of Ce3 and Ce6 are 0.244(6) and 0.300(6), respectively.

with symmetrical orientation, whereas Figure 5 shows the cage with unsymmetrical orientation. The shortest Ni-to-cage (carbon) distance is 2.71(3) or 2.73(3) Å depending on the cage orientation. Inside the cage, the cerium sites are disordered, and six partially occupied cerium sites have been identified either near or on the crystallographic mirror plane. The Ce–Ce distance in the pristine I_h-C_{80} cage ranges from 3.833 to 3.767 Å. This distance is shorter than the calculated value (3.850 Å)[11] but slightly longer than that in the isomeric D_{5h} cage (i.e., 3.764 Å as mentioned above). However, a longer Ce–Ce distance was found in a chemically modified cage, for instance, the Ce–Ce distance of 3.900 Å in $Ce_2@I_h$-$C_{80}(CH_2)_2NTrt$ (Trt = trityl),[9e] thus indicating the perturbation of appending moieties.

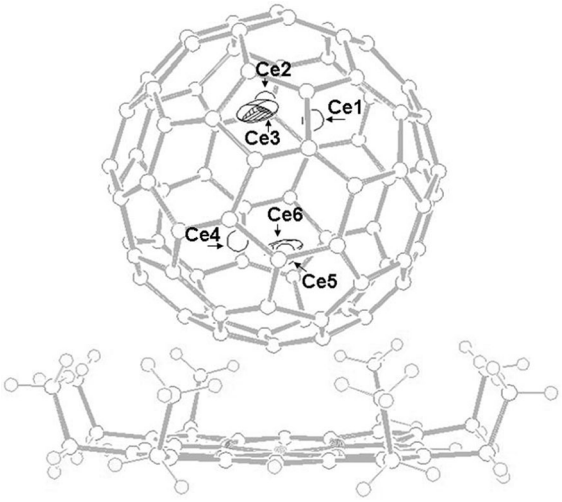

Figure 5. Drawing of $Ce_2@I_h$-C_{80} and Ni^{II}(OEP) showing only the cage with unsymmetrical orientation. In addition to Ce3 and Ce6A, another four cerium sites are also shown. Among them, sites Ce2 and Ce5 are on the crystallographic mirror plane with a separation of 3.833(13) Å, whereas site Ce4A is generated from site Ce4 by means of the mirror plane. Their occupancies are the following: Ce1 0.094(3), Ce2 0.324(10), Ce4 0.096(3), and Ce5 0.208(11). All cerium sites relative to each cage orientation are shown in Figures S2a and b in the Supporting Information, respectively.

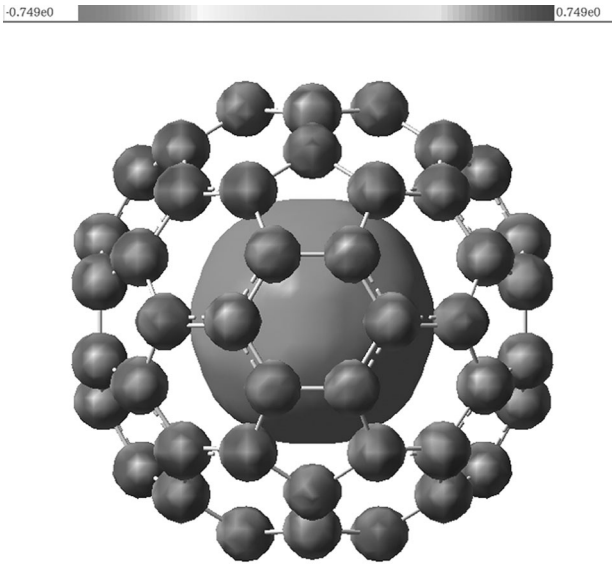

Figure 6. Electrostatic potential map of $(I_h$-$C_{80})^{6-}$ on the basis of the X-ray structure of $Ce_2@I_h$-C_{80}.

As shown in Figures 4, 5, and Figure S2 in the Supporting Information, at one end of the I_h-C_{80} cage, sites Ce2, Ce3, and Ce3A, which together correspond to 40.6% cerium content, are closely aligned under a hexagonal ring. Likewise, at another end of the I_h-C_{80} cage, sites Ce5, Ce6, and Ce6A, which correspond to a total of 40.4% cerium content, approach another hexagonal ring. The distribution of these major cerium sites similarly suggests an η^6 geometry of cerium–cage contact. In contrast, in $Ce_2@I_h$-$C_{80}(CH_2)_2$NTrt, the metal atoms are located under the carbon atoms shared by three hexagonal rings on the C_{80} cage rather than under hexagonal rings,[9e] thus indicating the remarkable influence of cage functionalization on the metal-to-cage contacts. Also, it appears that in the I_h-C_{80} cage the cerium cluster wanders in a swing way. With the major cerium sites, the molecule of $Ce_2@I_h$-C_{80} presents an approximate configuration of D_{2h}. This result stands in contrast to the recent theoretical prediction that the lowest-energy conformer of $Ce_2@I_h$-C_{80} is D_{3d},[13a] whereas it is consistent with that of $La_2@I_h$-C_{80}, which has a configuration of D_{2h}.[13b,c] Because a Ce atom has only one more f electron relative to an La atom, our result might suggest that this f electron has a negligible influence on the distribution on the lowest-energy conformer of $M_2@I_h$-C_{80}.

To check the cage–metal interaction further, the electrostatic potentials of $(I_h$-$C_{80})^{6-}$ were calculated on the basis of the X-ray structure of $Ce_2@I_h$-C_{80} and are mapped in Figure 6. However, it is hard to identify the localized electrostatic potential minima inside the I_h-C_{80} cage, which otherwise appears to be nearly delocalized, probably because this electrostatic potential well is too shallow or varies smoothly in this inner-cage space. A close inspection suggested that the difference among the cage radii, which are either close to or far from the Ce atom, is less remarkable, and the "punch-out" effect is hard to identify for this I_h-C_{80} cage. Also, unlike the D_{5h}-C_{80} cage, there are multiple cage motifs of ten contiguous hexagons on the I_h-C_{80} cage. Because all these cage motifs are equivalent, it is hard to conclude whether the major cerium sites are specifically along one of them. With regard to the presence of major cerium sites inside this I_h-C_{80} cage, an additional influence from Ni^{II}(OEP) was proposed. However, the theoretical calculation failed to present the origin of such influence and further studies will be necessary.

Conclusion

In summary, the dynamic cerium positions inside spherical C_{80} cages including D_{5h}-C_{80} and I_h-C_{80} have been characterized unambiguously by single-crystal X-ray diffraction studies. In particular, inside the D_{5h} cage, the primary cerium sites have been identified along a cage belt of ten contiguous hexagons, thus indicating significant influence of such a cage motif on the motion of the endohedral cluster. Further studies revealed a "punch-out" effect of the Ce_2 cluster, which induces a slightly distorted D_{5h} cage. Such geometrical distortion in turn results in the presence of two localized electrostatic potential minima inside $(D_{5h}$-$C_{80})^{6-}$, which agrees well with the major cerium sites, thereby reflecting the predominate ionic cerium–cage interactions. In contrast, inside the I_h cage, the motional behavior of the Ce_2 cluster is different from that in the D_{5h} cage. With the major metal sites, the molecule of $Ce_2@I_h$-C_{80} presents an approximate configuration of D_{2h}. Also, unlike the D_{5h} cage, the geometrical distortion and the localized electrostatic potential

minima are almost invisible for this I_h cage. We propose that a combined influence from not only the cage but also Ni^{II}-(OEP) might account for the limited cerium sites mapped inside the I_h cage. In addition, for both isomeric $Ce_2@C_{80}$, the major cerium sites generally sit under a hexagonal ring, thus indicating a preferable η^6 geometry of cerium-to-cage contact.

Experimental Section

The synthesis and isolation of $Ce_2@D_{5h}$-C_{80} and $Ce_2@I_h$-C_{80} were described in earlier studies.[11,14] Briefly, the dimetallofullerenes studied here were synthesized by using an improved arc-discharge method and isolated with multiple-stage high-performance liquid chromatography (HPLC) separations. The purity of all samples was estimated to be higher than 99% with both HPLC analysis and laser desorption time-of-flight mass spectrometry.

Black cocrystals of $Ce_2@D_{5h}$-C_{80} or $Ce_2@I_h$-C_{80} and Ni^{II}(OEP) were obtained by allowing a solution of fullerene in benzene and a solution of Ni^{II}(OEP) in chloroform to diffuse together. X-ray data were collected at 90 K by using a diffractometer (APEX II; Bruker Analytik GmbH) equipped with a CCD collector. The multiscan method was used for absorption correction. The structures were resolved using direct methods (SHELXS97) and refined on F^2 by using full-matrix least squares with SHELXL97.[15] In refinement, the intact cage was modeled by means of the crystallographic mirror plane. The sum of the occupancy factors for all cerium sites was set as 1.00, whereas the cage occupancy is 0.5. Hydrogen atoms were added geometrically and refined with a riding model.

The cocrystal of $Ce_2@D_{5h}$-C_{80}·Ni^{II}(OEP)·C_6H_6 contains a severely disordered lattice of C_6H_6 and $CHCl_3$ molecules that could not be modeled properly. Therefore, the SQUEEZE program, a part of the PLATON package of crystallographic software,[16] was used to calculate the solvent disorder area and remove its contribution from the intensity data.

Crystal data for $Ce_2@D_{5h}$-C_{80}·Ni^{II}(OEP)·C_6H_6: $C_{122}H_{50}Ce_2N_4Ni$, M_r = 1910.61; $0.30\times0.23\times0.21$ mm^3, monoclinic, $C2/m$; a = 25.2655(13), b = 15.0629(7), c = 19.7681(10) Å; β = 95.331(2)°; V = 7490.6(6) Å^3; Z = 4, ρ_{calcd} = 1.694 g cm^{-3}; $\mu(Mo_{K\alpha})$ = 1.510 mm^{-1}; θ = 1.03–27.48°; T = 90 K; R_1 = 0.0833, wR_2 = 0.1787 for all data; R_1 = 0.0764, wR_2 = 0.1754 for 8729 reflections ($I>2.0\sigma(I)$) with 867 parameters. Maximum residual electron density 2.357 e Å^{-3}.

Crystal data for $Ce_2@I_h$-C_{80}·Ni^{II}(OEP)·0.15 (C_6H_6)·1.85 ($CHCl_3$): $C_{118.75}H_{46.75}Ce_2Cl_{5.50}N_4Ni$, M_r = 2063.28; $0.25\times0.24\times0.20$ mm^3, monoclinic, $C/2m$; a = 25.138(3), b = 15.3226(18), c = 19.453(2) Å; β = 95.689(2)°; V = 7455.9(15) Å^3; Z = 4; ρ_{calcd} = 1.839 g cm^{-3}; $\mu(Mo_{K\alpha})$ = 1.716 mm^{-1}; θ = 1.56–25.02°; T = 90 K; R_1 = 0.0973, wR_2 = 0.2078 for all data; R_1 = 0.0804, wR_2 = 0.1942 for 6852 reflections ($I>2.0\sigma(I)$) with 915 parameters. Maximum residual electron density 1.266 e Å^{-3}.

More detailed crystal data are presented in Tables S1 and S2 in the Supporting Information. CCDC-863909 and -863910 contain the supplementary crystallographic data for this paper. These data can be obtained free of charge from The Cambridge Crystallographic Data Centre via www.ccdc.cam.ac.uk/data_request/cif.

The calculations were conducted using the hybrid density functional theory (DFT) at the B3LYP[17] level using the Gaussian 03 program.[18] The split-valence d-polarized 6-31G(d)[19] basis set was used for C. The relativistic effective core potential (ECP) and CEP-31G[20] basis sets were used for Ce.

Acknowledgements

This work was supported in part by a Grant-in-Aid for Scientific Research on Innovative Areas (no. 20108001, "π-Space"), a Grant-in-Aid for Scientific Research (A) (no. 20245006), (B) (no. 24350019), The Next Generation Super Computing Project (Nanoscience Project), the Nanotechnology Support Project, Grants-in-Aid for Scientific Research on Priority Area (nos. 20036008, 20038007), and Specially Promoted Research (no. 22000009) from the Ministry of Education, Culture, Sports, Science, and Technology of Japan, and The Strategic Japanese-Spanish Cooperative Program funded by JST and MICINN. F.L. also thanks NSF of Jiangsu Province of China (no. BK2012611).

[1] a) T. Akasaka, S. Nagase, *Endofullerenes: A New Family of Carbon Clusters*, Kluwer, Dordrecht, **2002**; b) T. Akasaka, F. Wudl, S. Nagase, *Chemistry of Nanocarbons*, Wiley, Chichester, **2010**; c) L. Feng, T. Akasaka, S. Nagase, In *Carbon Nanotubes and Related Structures* (Eds.: D. M. Guldi, N. Martin), Wiley-VCH, Weinheim, **2010**, pp. 455–490; d) X. Lu, T. Akasaka, S. Nagase, *Rare Earth Metals Trapped inside Fullerenes Endohedral Metallofullerenes. In Rare Earth Coordination Chemistry: Fundamentals and Applications* (Ed.: C. H. Huang), Wiley, Singapore, **2010**, pp. 273–308; e) X. Lu, T. Akasaka, S. Nagase, *Chem. Commun.* **2011**, *47*, 5942–5957.

[2] a) A. Stróżecka, K. Muthukumar, J. A. Larsson, A. Dybek, T. J. S. Dennis, J. Mysliveček, B. Voigtländer, *Phys. Rev. B* **2011**, *83*, 165414; b) Á. J. Pérez-Jiménez, *J. Phys. Chem. C* **2007**, *111*, 17640–17645.

[3] M. Yamada, T. Akasaka, S. Nagase, *Acc. Chem. Res.* **2010**, *43*, 92–102.

[4] B. Q. Mercado, A. Jiang, H. Yang, Z. Wang, H. Jin, Z. Liu, M. M. Olmstead, A. L. Balch, *Angew. Chem.* **2009**, *121*, 9278–9280; *Angew. Chem. Int. Ed.* **2009**, *48*, 9114–9116.

[5] C. M. Beavers, H. Jin, H. Yang, Z. Wang, X. Wang, H. Ge, Z. Liu, B. Q. Mercado, M. M. Olmstead, A. L. Balch, *J. Am. Chem. Soc.* **2011**, *133*, 15338–15341.

[6] a) X. Lu, H. Nikawa, T. Nakahodo, T. Tsuchiya, I. M. O. shitsuka, Y. Maeda, T. Akasaka, M. Toki, H. Sawa, Z. Slanina, N. Mizorogi, S. Nagase, *J. Am. Chem. Soc.* **2008**, *130*, 9129–9136; b) X. Lu, H. Nikawa, T. Tsuchiya, Y. Maeda, M. O. Ishitsuka, T. Akasaka, M. Toki, H. Sawa, Z. Slanina, N. Mizorogi, S. Nagase, *Angew. Chem.* **2008**, *120*, 8770–8773; *Angew. Chem. Int. Ed.* **2008**, *47*, 8642–8645.

[7] H. Yang, H. Jin, B. Hong, Z. Liu, C. M. Beavers, H. Zhen, Z. Wang, B. Q. Mercado, M. M. Olmstead, A. L. Balch, *J. Am. Chem. Soc.* **2011**, *133*, 16911–16919.

[8] a) M. M. Olmstead, A. de Bettencourt-Dias, S. Stevenson, H. C. Dorn, A. L. Balch, *J. Am. Chem. Soc.* **2002**, *124*, 4172–4173; b) M. M. Olmstead, H. M. Lee, S. Stevenson, H. C. Dorn, A. L. Balch, *Chem. Commun.* **2002**, 2688–2689.

[9] a) M. Yamada, T. Nakahodo, T. Wakahara, T. Tsuchiya, Y. Maeda, T. Akasaka, M. Kako, K. Yoza, E. Horn, N. Mizorogi, K. Kobayashi, S. Nagase, *J. Am. Chem. Soc.* **2005**, *127*, 14570–14571; b) M. Yamada, T. Wakahara, T. Nakahodo, T. Tsuchiya, Y. Maeda, T. Akasaka, K. Yoza, E. Horn, N. Mizorogi, S. Nagase, *J. Am. Chem. Soc.* **2006**, *128*, 1402–1403; c) T. Wakahara, M. Yamada, S. Takahashi, T. Nakahodo, T. Tsuchiya, Y. Maeda, T. Akasaka, M. Kako, K. Yoza, E. Horn, N. Mizorogi, S. Nagase, *Chem. Commun.* **2007**, 2680–2682; d) M. Yamada, C. Someya, T. Wakahara, T. Tsuchiya, Y. Maeda, T. Akasaka, K. Yoza, E. Horn, M. T. H. Liu, N. Mizorogi, S. Nagase, *J. Am. Chem. Soc.* **2008**, *130*, 1171–1176; e) M. Yamada, M. Okamura, S. Sato, C. I. Someya, N. Mizorogi, T. Tsuchiya, T. Akasaka, T. Kato, S. Nagase, *Chem. Eur. J.* **2009**, *15*, 10533–10542; f) M. Yamada, M. Minowa, S. Sato, M. Kako, Z. Slanina, N. Mizorogi, T. Tsuchiya, Y. Maeda, S. Nagase, T. Akasaka, *J. Am. Chem. Soc.* **2010**, *132*, 17953–17960; g) M. O. Ishitsuka, S. Sano, H. Enoki, S. Sato, H. Nikawa, T. Tsuchiya, Z. Slanina, N. Mizorogi, M. T. H. Liu, T. Akasaka, S. Nagase, *J. Am. Chem. Soc.* **2011**, *133*, 7128–7134; h) M. Yamada, M. Minowa, S. Sato, Z. Slanina, T. Tsuchiya, Y. Maeda, S. Nagase, T. Akasaka, *J. Am. Chem. Soc.* **2011**, *133*, 3796–3799.

[10] a) T. Cai, L. Xu, M. R. Anderson, Z. Ge, T. Zuo, X. Wang, M. M. Olmstead, A. L. Balch, H. W. Gibson, H. C. Dorn, *J. Am. Chem. Soc.* **2006**, *128*, 8581–8589; b) T. Zuo, C. M. Beavers, J. C. Duchamp, A. Campbell, H. C. Dorn, M. M. Olmstead, A. L. Balch, *J. Am. Chem. Soc.* **2007**, *129*, 2035–2043; c) T. Zuo, M. M. Olmstead, C. M.

Beavers, A. L. Balch, G. Wang, G. T. Yee, C. Shu, L. Xu, B. Elliott, L. Echegoyen, J. C. Duchamp, H. C. Dorn, *Inorg. Chem.* **2008**, *47*, 5234–5244.
[11] M. Yamada, N. Mizorogi, T. Tsuchiya, T. Akasaka, S. Nagase, *Chem. Eur. J.* **2009**, *15*, 9486–9493.
[12] R. C. Haddon, *Science* **1993**, *261*, 1545–1550.
[13] a) K. Muthukumar, J. A. Larsson, *J. Mater. Chem.* **2008**, *18*, 3347–3351; b) J. Zhang, C. Hao, S. M. Li, W. H. Ming, P. Jin, *J. Phys. Chem. C* **2007**, *111*, 7862–7867; c) A. A. Popov, L. Dunsch, *J. Am. Chem. Soc.* **2008**, *130*, 17726–17742.
[14] J. Ding, S. Yang, *Angew. Chem.* **1996**, *108*, 2369–2371; *Angew. Chem. Int. Ed. Engl.* **1996**, *35*, 2234–2235.
[15] G. M. Sheldrick, *Acta Crystallogr. Sect. A* **2008**, *64*, 112.
[16] a) A. L. Spek, "PLATON. A multipurpose crystallographic tool", Utrecht University, The Netherlands, **2003**; b) SQUEEZE: P. van der Sluis, A. L. Spek, *Acta Crystallogr. Sect. A* **1990**, *46*, 194–201.
[17] a) A. D. Becke, *Phys. Rev. A* **1988**, *38*, 3098–3100; b) A. D. Becke, *J. Chem. Phys.* **1993**, *98*, 5648–5652; c) C. Lee, W. Yang, R. G. Parr, *Phys. Rev. B* **1988**, *37*, 785–789.
[18] Gaussian 03 (Revision C.01), M. J. Frisch, G. W. Trucks, H. B. Schlegel, G. E. Scuseria, M. A. Robb, J. R. Cheeseman, G. Scalmani, V. Barone, B. Mennucci, G. A. Petersson, H. Nakatsuji, M. Caricato, X. Li, H. P. Hratchian, A. F. Izmaylov, J. Bloino, G. Zheng, J. L. Sonnenberg, M. Hada, M. Ehara, K. Toyota, R. Fukuda, J. Hasegawa, M. Ishida, T. Nakajima, Y. Honda, O. Kitao, H. Nakai, T. Vreven, J. A. Montgomery, Jr., J. E. Peralta, F. Ogliaro, M. Bearpark, J. J. Heyd, E. Brothers, K. N. Kudin, V. N. Staroverov, R. Kobayashi, J. Normand, K. Raghavachari, A. Rendell, J. C. Burant, S. S. Iyengar, J. Tomasi, M. Cossi, N. Rega, J. M. Millam, M. Klene, J. E. Knox, J. B. Cross, V. Bakken, C. Adamo, J. Jaramillo, R. Gomperts, R. E. Stratmann, O. Yazyev, A. J. Austin, R. Cammi, C. Pomelli, J. W. Ochterski, R. L. Martin, K. Morokuma, V. G. Zakrzewski, G. A. Voth, P. Salvador, J. J. Dannenberg, S. Dapprich, A. D. Daniels, Ö. Farkas, J. B. Foresman, J. V. Ortiz, J. Cioslowski, D. J. Fox, Gaussian, Inc., Wallingford CT, **2003**.
[19] P. C. Hariharan, J. A. Pople, *Theor. Chim. Acta* **1973**, *28*, 213–222.
[20] T. R. Cundari, W. J. Stevens, *J. Chem. Phys.* **1993**, *98*, 5555–5565.

Received: July 1, 2012
Published online: December 19, 2012

